used to investigate IPV effect performance improvements in solar cells for any promising candidate impurity.

Specifically, we have applied the approach to indium as the IPV impurity incorporated into an ideal silicon solar cell. The calculations are based on reported experimental parameters for indium in silicon. The rate-limiting step for electron-hole pair creation via indium is the electron photoemission process, since hole emission is strong and provided thermally. We use two models to represent upper and lower bounds on this cross section. The solar cell considered is assumed electronically ideal in that it has long diffusion lengths, perfect surface passivation, and infinite carrier mobilities. Optically, it has a randomising light trapping scheme and can have perfect rear reflectivity. Our calculations therefore represent upper limits for the IPV improvements of indium. However, the results are also related, with qualification, to present high efficiency silicon solar cells.

Our work reveals the importance of light trapping and the need to have indium approximately compensated by an n-type dopant. Compensating the indium keeps it fully occupied. This keeps the rate-determining electron photoemission process supplied with bound electrons, suppresses recombination via the indium level, and suppresses absorption of photons by the non-crucial hole photoemission process. If the latter process is not minimised, it competes not only with the electron photoemission from the indium, but also with e-h pair creation by intrinsic band-to-band absorption.

Our calculations show that significant short-circuit current improvements (up to 5mA/cm^2) result from indium incorporation, provided there is good light trapping, the indium concentration is at least about 10^{17}cm^{-3}, and the indium is close to compensation by an n-type dopant. Spectral response calculations confirm that such improvements are due to extension of the long wavelength response into the sub-bandgap region, and they also indicate that spectral response measurements are able to improve experimental data on the optical cross section for photoemission from the indium level. Indium incorporation, even under the most favourable conditions, reduces the open-circuit voltage of our model cell because of indium's role as a recombination centre at high operating voltages. However, such reductions are outweighed by the improvements of the cell short-circuit current. Indium incorporation indeed significantly improves cell energy conversion efficiency, by as much as 1 to 2% absolute. This is the first time that the IPV effect is shown to improve solar cell efficiency.

ACKNOWLEDGEMENTS

The Centre for Photovoltaic Devices and Systems is funded by the Australian Research Council's Special Research Centres Scheme and by Pacific Power. The first author would like to thank members of the Centre, in particular Armin Aberle, for helpful discussions.

[1] M. Wolf, "Limitations and Possibilities for Improvement of Photovoltaic Solar Energy Converters", *Proc. IRE* **48**, 1246 (1960).

[2] G. Güttler and H. J. Queisser, "Impurity Photovoltaic Effect in Silicon", Energy Conversion **10**, 51 (1970).

[3] J. Li, M. Chong, J. Zhu, Y. Li, J. Xu, P. Wang, Z. Shang, Z. Yang, R. Zhu X. Cao, "35% efficient nonconcentrating novel silicon solar cell", Appl. Phys. Lett. **60**, 2240 (1992).

[4] M. A. Green, *High Efficiency Silicon Solar Cells,* (Trans. Tech. Publications, Aedermannsdorf, 1987).

[5] M. J. Keevers and M. A. Green, "The Impurity Photovoltaic Effect for Indium-doped Silicon Solar Cells with Light Trapping", Internal Report (1992/01), Centre for Photovoltaic Devices and Systems, UNSW, June 1992.

[6] Y.K. Hsieh, H.C. Card, "Limitation to Shockley-Read-Hall model due to direct photoionization of the defect states", J. Appl. Phys. **65**, 2409 (1989).

[7] M. A. Green, "Intrinsic Concentration, Effective Densities of States, and Effective Mass in Silicon", J. Appl. Phys. **67**, 2944 (1990).

[8] R. I. Chikovani, Y. E. Pokrovskii, "Determination of the Photoionization Cross Section of Negatively Charged Indium Atoms in Silicon", Sov. Phys. Solid State **8**, 1856 (1967).

[9] B. O. Sunstrom, L. Huldt, N. G. Nilsson, "Electron Capture Coefficient of Neutral Indium and Pair Recombination in Compensated Silicon", J. Phys. C**15**, 3359 (1982).

[10] H. M. Hobgood, T. T. Braggins, M. M. Sopira, J. C. Swartz and R. N. Thomas, "Growth and Characterization of Indium-Doped Silicon for Extrinsic IR Detectors", IEEE Trans. Electron Devices, **ED-27**, 14 (1980).

[11] D. Margadonna, F. Ferrazza, R. Peruzzi, "Donor and Acceptor Neutralization in Multicrystalline Silicon", Proc. of 10th European Photovoltaic Solar Energy Conference, Lisbon, Portugal, 1991, p.678.

[12] X. M. Dai, M. A. Green and S. R. Wenham, "High Efficiency n-Silicon Solar Cells using Rear Junction Structures", Conf. Rec. 23rd IEEE Photovoltaic Specialists Conf., Louisville, Kentucky, May, 1991.

[13] R. A. Sinton, R. R. King and R. M. Swanson, "Novel Implementations of Backside-Contact Silicon Solar Cell Designs in One-Sun and Concentrator Applications", Proc. of 4th International Photovoltaic Science and Engineering Conference, Sydney, Australia, 1989, p. 143.

[14] P.A. Basore, "PC-1D Version 3: Improved Speed and Convergence", Conf. Rec. 22nd IEEE Photovoltaic Spec. Conf., Las Vegas, October, 1991, p. 299.

EXTENDED SPECTRAL ANALYSIS OF INTERNAL QUANTUM EFFICIENCY

Paul A. Basore
Sandia National Laboratories
Albuquerque, NM 87185-5800

ABSTRACT

A powerful new method for identifying the performance-limiting mechanisms in silicon cells has been developed and tested at Sandia. This method uses the internal quantum efficiency (IQE) of the device at both near-infrared and near-bandgap wavelengths. The conventional interpretation of IQE is expanded to accommodate textured surfaces and long diffusion lengths, and extended to near-bandgap wavelengths where internal optical effects play an important role. This paper describes how the information available from this extended analysis can be used to obtain a value for the internal optical reflectance of the back surface, and to separate the effects of diffusion length from back-surface recombination. Results from experimental tests verify the method. The information obtained can be used to compute recombination components for the cell, and to quantify the light-trapping effectiveness of the device.

INTRODUCTION

The absorption coefficient for monochromatic light in silicon is a strong function of wavelength, so the spectral response of silicon solar cells contains information about their internal operation. But to study the internal operation, it is first necessary to eliminate external optical effects from the spectral response data. This can be accomplished by measuring the total hemispherical reflectance of the cell as a function of wavelength. The spectral response can be adjusted to account for the optical reflectance, yielding the internal quantum efficiency (IQE) of the device. Specifically, IQE is calculated at each wavelength from the measured spectral response, SR(λ) (amps/watt), and hemispherical reflectance, R(λ), using:

$$IQE = SR \cdot (hc/q\lambda)/(1-R), \qquad (1)$$

where λ is the free-space wavelength and hc/q = 1239.84 V·nm. IQE is intended to represent the fraction of the minority carriers photogenerated in the cell that are collected under short-circuit conditions. But, in practice, the measurement fails to accurately represent this concept because it cannot distinguish between carrier-producing absorption in the silicon and parasitic absorption. Parasitic absorption of photons at the back surface is particularly important for weakly absorbed wavelengths near the bandgap. This effect can be exploited to obtain information about the internal reflectance of the back surface [1].

This work supported by the Photovoltaics Technology Division, U.S. Department of Energy, contract DE-AC04-76DP00789.

The conventional interpretation of IQE data is obtained from a plot of IQE^{-1} versus α^{-1}, where the optical absorption coefficient, α, is a known function of wavelength [2]. For planar cells of thickness W with a diffusion length, L, much shorter than the thickness, the plot is linear for absorption lengths (α^{-1}) greater than the junction depth but shorter than the device thickness. The inverse of this slope is equal to the minority-carrier diffusion length in the base region.

The analysis of IQE data can be extended to accommodate textured surfaces, long diffusion lengths, and weakly absorbed light. Fig. 1 illustrates the optical model on which the method described in this paper is based. Incident light is partially reflected at the external front surface (R_{fe}). That which gets into the silicon is refracted to an angle θ_1 by the front-surface texture. For chemically textured (100)-oriented silicon, this angle is 41.8° for $\lambda \approx 900$ nm. If the energy of the photons is near the bandgap of silicon, some fraction of the light (T_1) will be transmitted to the back surface of the cell, where it will be partially reflected back toward the front of the cell (R_{b1}). If the rear surface is polished, these reflected rays will retain the same path angle on their return trip (θ_2). But if the rear surface is rough, the rays will be at least partially randomized in their return orientation. When the reflected light is completely randomized, the effective path angle is 60°. Partially randomized light will have a smaller effective path angle.

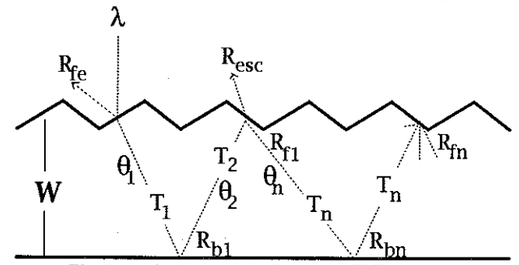

Fig. 1. Optical Model for Extended IQE Analysis.

A portion of the reflected light (T_2) will reach the internal front surface of the cell. Some of this light will escape out the front, contributing to the measured hemispherical reflectance (R_{esc}); the rest will be reflected back inside for another pass (R_{f1}). Any rays that remain trapped inside the cell at this point are probably completely random in their orientation. They will continue to bounce back and forth, with a certain transmittance

0-7803-1220-1/93 $3.00 © 1993 IEEE

each pass (T_n), and with successive internal reflectances at back (R_{bn}) and front (R_{fn}) surfaces.

paper will describe how this optical model can be used to act information from the spectral dependence of internal ntum efficiency. Equations are presented which incorporate f the parameters of this model. A sensitivity analysis of the del was used to identify which parameters have the greatest ct on the measured data. Only a few parameters are shown e important, allowing data interpretation to be simplified ificantly. Finally, the method is verified by evaluating cells icated at Sandia under controlled conditions designed to only one cell parameter at a time.

THE DATA

data has been collected in Sandia's Photovoltaic Device asurement Laboratory for more than a decade. Recently, the dware used for the spectral response measurement has been nificantly improved. The absolute accuracy of this system is rently estimated at better than ±2% for wavelengths ween 400 and 1120 nm. IQE has since been measured on re than 100 cells using this new system. Plots of inverse-IQE sus absorption length for the wavelength range 800 nm to 20 nm have consistently displayed two linear regimes, as strated in Fig. 2 for a textured high-performance silicon cell ricated at Sandia.

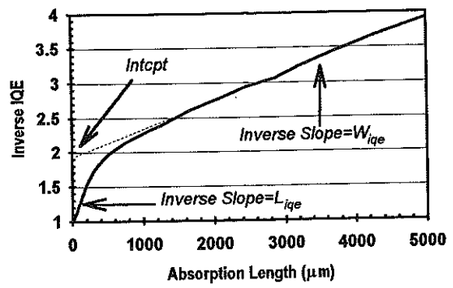

ig. 2. Typical Inverse-IQE data showing two linear regimes.

e first linear regime occurs at near-infrared wavelengths. is is the data conventionally used to interpret IQE. But, for a xtured cell such as this one, the inverse slope, L_{iqe}, cannot be rectly equated to the diffusion length. The second linear gime occurs at near-bandgap wavelengths. The existence of e second linear regime was first predicted using the computer ogram PC-1D [4]. The inverse slope of this region, W_{iqe}, and e extrapolated intercept of this line with the axis, Intcpt, form e basis for an "extended IQE analysis."

THE EQUATIONS

ne numerator of equation (1) can be expressed as the product the fraction of the incident photons that are absorbed (f_{abs}) mes the probability that the carriers generated by this sorption are successfully collected at the junction (η_c):

$$IQE = f_{abs}\eta_c / (1-R). \tag{2}$$

The optical model of Fig. 1 can be used to derive expressions for f_{abs} and R, while an electrical model is needed to determine an expression for η_c.

Optical Model Equations

The fraction of the incident light absorbed in the cell, excluding parasitic absorption at the back surface, is

$$f_{abs} = (1-R_{fe})\left\{\frac{(1-T_1)+R_{b1}T_1(1-T_2)}{+\dfrac{R_{b1}R_{f1}T_1T_2(1-T_n)(1+R_{bn}T_n)}{1-R_{bn}R_{fn}T_n^2}}\right\}. \tag{3}$$

The total reflectance, including escape reflectance, is given by

$$1-R = (1-R_{fe})\left\{\frac{1-R_{b1}T_1T_2(1-R_{f1})}{-\dfrac{R_{b1}R_{f1}T_1T_2R_{bn}(1-R_{fn})T_n^2}{1-R_{bn}R_{fn}T_n^2}}\right\}. \tag{4}$$

Electrical Model Equations

The electrical model used in this work is a simple one. The base region of the cell is a quasi-neutral region in low-level injection, characterized by a uniform minority-carrier diffusion length (L) and diffusivity (D), and a surface recombination velocity (S) at the back surface. The collecting junction is assumed to be located at the front surface. The wavelength range considered is restricted to λ>800 nm so that the influence of recombination in the thin emitter region can be neglected.

Despite this simple model, an analytical expression valid over the entire wavelength range would be extraordinarily complex, because the photogeneration profile in the device is affected by light trapping at the longer wavelengths. However, simple expressions can be obtained in two limiting cases: (1) for near-infrared wavelengths unaffected by light trapping, and (2) at near-bandgap wavelengths where photogeneration is uniform throughout the device.

For near-infrared wavelengths, the product αW is much greater than 1, so none of the photons penetrate to the back surface. The fraction of the photogenerated carriers that are collected under short-circuit conditions, η_c, is a function of wavelength because it depends on the absorption depth of the light [3]. For a planar surface, the collection efficiency in this limit is:

$$\eta_c = \frac{\alpha L}{\alpha^2L^2-1}\left\{\alpha L - \frac{SL/D + \tanh W/L}{1+SL/D\tanh W/L}\right\}. \tag{5}$$

With a textured surface, the only difference is that the light traverses the cell at an angle θ_1, so that it is necessary to replace α in equation (5) with $\alpha/\cos\theta_1$. Equation (5) can be

simplified by considering its behavior for different values of L. When L<<W, the expression in brackets reduces to {αL-1}. When L is comparable to or greater than W, unity terms can be ignored compared to terms of the order α^2L^2, because of the initial premise that αW>>1 (hence αL>>1).

For near-bandgap wavelengths, light is absorbed slowly and photogeneration occurs uniformly throughout the device. The fraction of the generated carriers that are collected under short-circuit conditions, η_c, becomes independent of wavelength [4]:

$$\eta_c = \frac{L}{W}\cdot\frac{SL/D + \tanh W/L - \dfrac{SL/D}{\cosh W/L}}{1+SL/D\tanh W/L}. \tag{6}$$

IQE Equation for Near-Infrared Wavelengths

For wavelengths that do not penetrate to the rear surface, equation (3) gives the expected result that f_{abs}=1-R_{fe}. In silicon, the range of wavelength where this limit applies is approximately 800 nm to 1000 nm. Incorporating the simplifications mentioned for equation (5), a single expression for inverse-IQE at near-infrared wavelengths can be written that is valid for all values of L:

$$IQE^{-1} = 1+\frac{\cos\theta_1}{\alpha L_{eff}}, \tag{7}$$

where

$$L_{eff} = L\cdot\frac{1+SL/D\tanh W/L}{SL/D+\tanh W/L}. \tag{8}$$

Equation (7) predicts a linear dependence of inverse-IQE on absorption length, just as in the conventional interpretation of IQE, but with inverse slope $L_{iqe}=L_{eff}/\cos\theta_1$ in place of L. It is quite useful to note that L_{eff} as defined in equation (8) is the same effective diffusion length that determines the base component of the dark saturation current density:

$$J_{ob} = \frac{qDn_i^2}{N_BL_{eff}}, \tag{9}$$

where N_B is the base doping density and n_i is the intrinsic carrier concentration (n_i=8.6x10^9 cm^{-3} for Si at 25°C).

IQE Equation for Near-Bandgap Wavelengths

For wavelengths that are only weakly absorbed, the wavelength dependence of IQE derives not from the electrical collection efficiency, but rather from the optical absorptance. The expressions for f_{abs} and 1-R given in equations (3) and (4) can be inserted into the expression for IQE given in equation (2) to obtain the following rather complicated expression for inverse IQE in the near-bandgap wavelength range:

$$IQE^{-1} = \frac{1}{\eta_c}\cdot\frac{[1-R_{b1}T_1T_2(1-R_{f1})][1-R_{bn}R_{fn}T_n^2]}{\begin{matrix}-R_{b1}R_{f1}T_1T_2R_{bn}(1-R_{fn})T_n^2\\ [(1-T_1)+R_{b1}T_1(1-T_2)][1-R_{bn}R_{fn}T_n^2]\\ +R_{b1}R_{f1}T_1T_2(1-T_n)(1+R_{bn}T_n)\end{matrix}}. \tag{10}$$

In silicon, the wavelength range over which this expression is appropriate is approximately 1080 nm to 1120 nm. At shorter wavelengths the absorption is not spatially uniform. At longer wavelengths the absorption coefficient is too uncertain, being affected by free-carrier absorption and temperature-induced variation in the bandgap.

The dominant wavelength dependence of equation (10) lies in the transmittances T_1, T_2, and T_n, where

$$T_1 = e^{-\alpha W/\cos\theta_1},\ T_2 = e^{-\alpha W/\cos\theta_2},\ T_n = e^{-\alpha W/\cos\theta_n}. \tag{11}$$

For weakly absorbed light, the transmittances in equation (11) can be expressed as an infinite series involving powers of α. The numerator and denominator of equation (10) can, in turn, be expressed as two power series involving α:

$$IQE^{-1} = \frac{1}{\eta_c}\cdot\frac{a_0+a_1(\alpha W)+a_2(\alpha W)^2+\ldots}{b_0+b_1(\alpha W)+b_2(\alpha W)^2+\ldots}, \tag{12}$$

The denominator term b_0 is equal to zero; so that, for small α, the two largest terms in the expression for IQE^{-1} are of the order α^{-1} and α^0. This corresponds to the anticipated linear dependence of inverse-IQE on inverse absorption coefficient:

$$IQE^{-1} \cong \frac{1}{\eta_c}\cdot\left\{\frac{a_1b_1-a_0b_2}{b_1^2}+\frac{a_0}{b_1}(\alpha W)^{-1}\right\}, \tag{13}$$

where

$$a_0 = [1-R_{b1}(1-R_{f1})][1-R_{bn}R_{fn}]-R_{b1}R_{bn}R_{f1}(1-R_{fn}),$$

$$a_1 = R_{b1}[1-R_{f1}-R_{bn}(R_{fn}-R_{f1})][1/\cos\theta_1 + 1/\cos\theta_2]$$
$$+2\{R_{fn}-R_{b1}(R_{fn}-R_{f1})][R_{bn}/\cos\theta_n],$$

$$b_1 = [1/\cos\theta_1 + R_{b1}/\cos\theta_2][1-R_{bn}R_{fn}]+R_{b1}R_{f1}(1+R_{bn})/\cos\theta_n,$$

$$b_2 = \begin{matrix}2R_{bn}R_{fn}/(\cos\theta_1\cos\theta_n) - 0.5(1-R_{bn}R_{fn})/\cos^2\theta_1\\ +2R_{b1}R_{bn}R_{fn}/(\cos\theta_2\cos\theta_n) - R_{b1}(1-R_{bn}R_{fn})/(\cos\theta_1\cos\theta_2)\\ -0.5R_{b1}(1-R_{bn}R_{fn})/\cos^2\theta_2 - R_{b1}R_{f1}R_{bn}/\cos^2\theta_n\\ -R_{b1}R_{f1}(1+R_{bn})[1/(\cos\theta_1\cos\theta_n) + 1/(\cos\theta_2\cos\theta_n)]\\ -0.5R_{b1}R_{f1}(1+R_{bn})/\cos^2\theta_n.\end{matrix}$$

n the linear dependence of IQE^{-1} on α^{-1} demonstrated in ation (13), the expressions for W_{iqe} and Intcpt are:

$$W_{iqe} = \eta_c W \frac{b_1}{a_0}, \qquad Intcpt = \frac{1}{\eta_c} \cdot \frac{a_1 b_1 - a_0 b_2}{b_1^2}. \tag{14}$$

e that the product W_{iqe}·Intcpt eliminates η_c. This product ends only on the optical properties of the cell, and is pendent of the cell's electrical properties!

iliary Optical Definitions

o commonly encountered parameters when discussing light ping in silicon cells are the light-trapping effectiveness or, Z [5], and the sub-bandgap reflectance, R_{sub}. The cal model presented in this paper can be used to derive ytical expressions for these two quantities.

Z factor for near-bandgap wavelengths is defined here as a kness multiplier for uniformly absorbed wavelengths:

$$Z = \frac{\lim_{\alpha \to 0} f_{abs}}{(1-R_{fe})\alpha W} = \frac{b_1}{1-R_{bn}R_{fn}}, \tag{15}$$

re b_1 is from equation (13). The sub-bandgap reflectance is n equation (4), by setting $T_1=T_2=T_n=1$:

$$1-R_{sub} = \frac{(1-R_{fe})a_0}{1-R_{bn}R_{fn}}, \tag{16}$$

re a_0 is also from equation (13). Note that

$$Z = \frac{b_1}{a_0} \cdot \frac{(1-R_{sub})}{(1-R_{fe})} = \frac{W_{iqe}}{\eta_c W} \cdot \frac{(1-R_{sub})}{(1-R_{fe})}. \tag{17}$$

SENSITIVITY ANALYSIS

value of W_{iqe}·Intcpt depends only on the optical meters of the cell. But the optical model for near-bandgap elengths involves far more parameters than can be found g IQE data alone. A sensitivity analysis was performed to rmine which optical parameters have the greatest effect on e·Intcpt. This analysis was performed for several different s of cells. The results of the analysis are shown in Table I a textured cell, and in Table II for a cell with a planar front ace but a rough rear surface. The values of the optical meters used to describe each cell are listed in the tables.

topology of the cell provides, by itself, some information ut the optical parameters. This *a priori* knowledge is listed ne tables as the pre-data uncertainty for each parameter. The ct of each optical parameter on the dimensionless factor e·Intcpt/W was calculated and is expressed in the tables as

TABLE I
SENSITIVITY ANALYSIS: TEXTURED CELL
R_{fl}=.7, R_{fn}=.92,R_{b1}=.7,R_{bn}=.7,cosθ_1=.75,cosθ_2=.65,cosθ_n=.5

Optical Parameter		W_{iqe}·Intcpt/W		Post-Data
Symbol	Pre-Data Uncertainty	Sensitivity Factor	Pre-Data Uncertainty	Parameter Uncertainty
R_{fl}	25%	+0.06	2%	25%‡
R_{fn}	5%	+0.25	1%	5%
R_{b1}	30% (5%)†	+0.45	14%	5%
R_{bn}	30%	**+2.51**	**75%**	3%
cosθ_1	10%	-0.03	0%	10%
cosθ_2	20%	-0.07	1%	20%
cosθ_n	5%	-0.89	4%	5%

†Because $R_{b1} \approx R_{bn}$, the smaller value applies if R_{bn} is known.
‡The uncertainty in R_{fl} can be reduced to 13% by measuring the sub-bandgap reflectance and using equation (16).

TABLE II
SENSITIVITY ANALYSIS: PLANAR CELL
R_{fl}=.6, R_{fn}=.92,R_{b1}=.7,R_{bn}=.7,cosθ_1=1,cosθ_2=.75,cosθ_n=.5

Optical Parameter		W_{iqe}·Intcpt/W		Post-Data
Symbol	Pre-Data Uncertainty	Sensitivity Factor	Pre-Data Uncertainty	Parameter Uncertainty
R_{fl}	50%	+0.09	4%	50%‡
R_{fn}	10%	+0.41	4%	10%
R_{b1}	30% (5%)†	+0.47	14%	5%
R_{bn}	30%	**+2.53**	**76%**	5%
cosθ_1	5%	-0.01	0%	5%
cosθ_2	30%	-0.07	2%	30%
cosθ_n	10%	-0.90	9%	10%

†Because $R_{b1} \approx R_{bn}$, the smaller value applies if R_{bn} is known.
‡The uncertainty in R_{fl} can be reduced to 20% by measuring the sub-bandgap reflectance and using equation (16).

a sensitivity coefficient — the percent change in the factor for a 1% change in the corresponding optical parameter. The pre-data uncertainty listed in the tables for W_{iqe}·Intcpt/W is just the product of the pre-data uncertainty in each parameter times the sensitivity of W_{iqe}·Intcpt/W to that parameter. This indicates how much additional uncertainty would be introduced if the *a priori* value of that parameter was assumed in the model. From this column it is quite clear that for both types of cells illustrated, the factor W_{iqe}·Intcpt/W is completely dominated by R_{bn}. Even if inaccurate *a priori* assumptions are made for all other optical parameters, it is still possible to

determine an accurate value for R_{bn} directly from the measured value of W_{iqe}·Intcpt/W. The dependence of this factor on R_{bn} is shown in Fig. 3 for the two types of cells considered.

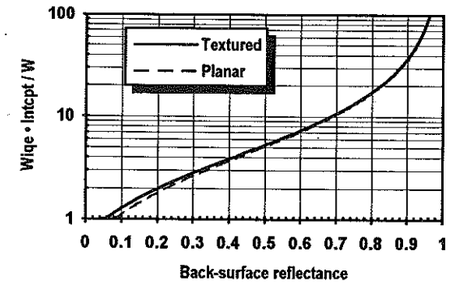

Fig. 3. Graphical representation showing how R_{bn} can be determined directly from the measured value of W_{iqe}·Intcpt/W.

The value obtained for R_{bn} using Fig. 3 has an estimated uncertainty of 5% or less, as listed in the tables. This estimate is obtained by assuming that W_{iqe}·Intcpt/W has its own measurement uncertainty of 5%, which is increased (using root-sum-squares) by the uncertainties in W_{iqe}·Intcpt/W due to having assumed values for all of the optical parameters other than R_{bn}. This total uncertainty in W_{iqe}·Intcpt/W, approximately 10%, is divided by the model's sensitivity to R_{bn} to obtain the post-data uncertainty listed in the table for R_{bn}.

A similar sensitivity analysis was conducted for the electrical collection efficiency, η_c. The collection efficiency is approximately equal to 1/Intcpt, with some influence from the parameters R_{b1} and R_{bn}. Since usually $R_{b1} \approx R_{bn}$, and R_{bn} is known to within 5% from Fig. 3, it is possible to determine η_c with similar accuracy: ±4% for the textured cell and ±8% for the planar cell. Fig. 4 illustrates the dependence of the product η_c·Intcpt on the back-surface reflectance.

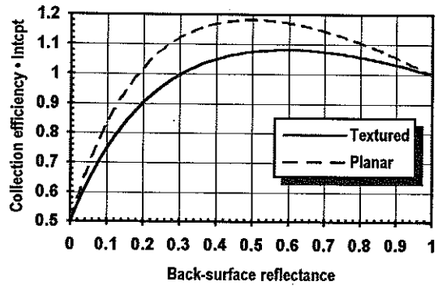

Fig. 4. Graphical representation showing how R_b and Intcpt can be used to determine η_c, for two different cell types.

The model presented here does not consider parasitic optical absorption other than at the back surface. If a cell with parasitic absorption at the front surface is evaluated using this model, the effect will be an apparent reduction in the value of R_{bn}.

SEPARATING THE EFFECT OF S FROM L

The relative significance of bulk recombination versus back-surface recombination can be evaluated by combining the results from the near-infrared wavelengths with results from the near-bandgap analysis. L_{eff}/W provides one relationship between the dimensionless electrical parameters L/W and SW/D. The collection efficiency, η_c, provides a different relationship between L/W and SW/D. In principle, equations (6) and (8) can be solved together to obtain both L and S. But not every combination of L_{eff}/W and η_c is physically possible. This constraint is clarified by Fig. 5, in which the cross-hatched area shows the parameter space that can satisfy both equations.

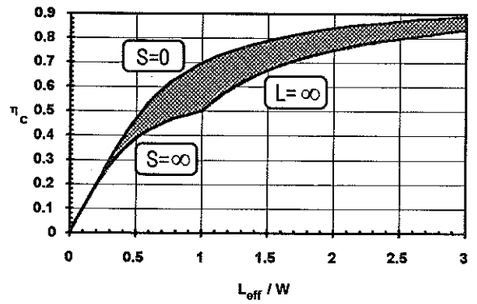

Fig. 5. Range of possible combinations of L_{eff}/W and η_c. No finite combination of L and S yields results outside this range.

In the lower-left corner of the parameter space shown in Fig. 5, L<<W. Here L dominates and can be found accurately, but no information is available regarding S. In the upper-right corner, recombination in the bulk and at the back surface are both small. The upper curve represents bulk-dominated recombination, while the lower curve represents surface-dominated recombination. In this region, the uncertainty inherent in η_c makes it possible only to determine whether one recombination mechanism is dominant, and if so which one. In the cross-hatched area near the center of the figure, the two equations can be solved to obtain meaningful values for both L and S, with greater accuracy for the dominant factor.

EXPERIMENTAL VERIFICATION

Extended IQE analysis has been applied to a wide variety of silicon cells over the past year, using spectral response and reflectance data from Sandia's Photovoltaic Device Measurement Laboratory. The method has been particularly useful for characterizing high-performance cells which combine long diffusion lengths with light trapping.

The most comprehensive tests of the method have been performed on cells prepared in Sandia's Photovoltaic Device Fabrication Laboratory under carefully controlled conditions. One test involved the coprocessing of cells with and without

PDFL Lot BL1-10 Wafers: 10 Ωcm p-type Si, W=640 μm, Aluminum Rear

ce	$L_{iqe}(\mu m)$	$L_{eff}(\mu m)$	$W_{iqe}(\mu m)$	Intcpt	R_{bn}	η_c
r	260	260	2370	2.50	66%	43%
red	345	260	2300	2.45	65%	44%

TABLE IV
Experimental Comparison of Back-Surface Metals
PDFL Lot BL1-11 Wafers: 2 Ωcm p-type Si, W=460 μm, Textured

Metal	$L_{iqe}(\mu m)$	$L_{eff}(\mu m)$	$W_{iqe}(\mu m)$	Intcpt	R_{bn}	η_c
inum	273	205	1930	2.23	67%	48%
ium	256	192	390	1.50	9%	48%

TABLE V
Experimental Evaluation of Al BSF on Different Wafer Materials
PDFL Lot BL1-21 Wafers: p-type Si, Textured, Aluminum-Alloy Rear

rial	W(μm)	$L_{eff}(\mu m)$	$W_{iqe}(\mu m)$	Intcpt	R_{bn}	η_c	L(μm)	S(cm/s)
m	470	380	2780	1.80	69%	60%	350	400
cm	585	600	3760	1.61	69%	67%	540	200

ical front-surface texturing. Both cell types received the back-surface aluminum evaporation. Despite substantial rences in spectral response and reflectance for these two , the internal parameters deduced are nearly identical, as d in Table III. In a second test, textured cells were tically prepared except that the back metal was either inum or titanium. According to the analysis, only the back ctance was significantly affected, as shown in Table IV. A l test was performed which subjected two different wafer erials to identical processing. Table V lists the parameters were extracted from these cells, including estimates of L S. Both materials received the same aluminum-alloy back-ace treatment, and the analysis reveals nearly identical c-surface reflectance, despite significant differences in usion length and wafer thickness.

CONCLUSIONS

lysis of internal quantum efficiency data has been extended near-infrared wavelengths to accommodate textured cells long diffusion lengths. The slope of the inverse IQE plot in wavelength range gives the effective diffusion length ded to calculate the base component of the saturation ent density to within about 5%. If the total saturation ent density is known from dark I-V or I_{sc}-V_{oc} data, one can ess the relative importance of the base versus the emitter in ermining the cell's voltage.

additional information available from near-bandgap velengths permits the determination of the internal back-face reflectance and the carrier collection efficiency for form photogeneration, to within about 5%. By combining the effective diffusion length from the near-infrared wavelengths with the collection efficiency from the near-bandgap wavelengths, it is possible to identify whether the dominant recomination mechanism in the base region of the cell is in the bulk or at the back surface.

Our experience at Sandia over the past year indicates that the extended-IQE analysis described here is the most reliable method yet devised for identifying the performance-limiting mechanisms in silicon solar cells, especially those which combine long diffusion lengths and light trapping. Most importantly, IQE analysis is performed nondestructively, on finished cells, using data that directly reflects the cell's performance.

REFERENCES

[1] James M. Gee, "The Effect of Parasitic Absorption Losses on Light Trapping in Thin Silicon Solar Cells," *20th IEEE PVSC* (September 1988), p. 549.

[2] Martin A. Green, *High Efficiency Silicon Solar Cells*, Trans Tech Publications, Switzerland, 1987, Appendix C.

[3] S.M. Sze, *Physics of Semiconductor Devices*, 2nd Ed., John Wiley & Sons, New York, 1981, p. 803.

[4] Paul A. Basore, "Numerical Modeling of Textured Silicon Solar Cells Using PC-1D," *IEEE Trans. on Electron Devices*, ED-37 (February 1990), p. 337.

[5] James A. Rand and Paul A. Basore, "Light-Trapping Silicon Solar Cells: Experimental Results and Analysis," *22nd IEEE PVSC* (October 1991), p. 192.